PHYSICAL REVIEW B **80**, 125203 (2009)

Ab initio theory of the lattice thermal conductivity in diamond

A. Ward and D. A. Broido
Department of Physics, Boston College, Chestnut Hill, Massachusetts 02467, USA

Derek A. Stewart
Cornell Nanoscale Facility, Cornell University, Ithaca, New York 14853, USA

G. Deinzer
Institut für theoretische Physik, Universität Regensburg, D-93040 Regensburg, Germany

(Received 4 June 2009; revised manuscript received 13 August 2009; published 16 September 2009)

We present a first-principles theoretical approach to calculate the lattice thermal conductivity of diamond based on an exact solution of the Boltzmann transport equation. Density-functional perturbation theory is employed to generate the harmonic and third-order anharmonic interatomic force constants that are required as input. A central feature of this approach is that it provides accurate representations of the interatomic forces and at the same time introduced no adjustable parameters. The calculated lattice thermal conductivities for isotopically enriched and naturally occurring diamond are both in very good agreement with experimental data. The role of the scattering of heat-carrying acoustic phonons by optic branch phonons is also investigated. We show that inclusion of this scattering channel is indispensable in properly describing the thermal conductivity of semiconductors and insulators. The accurate adjustable-parameter-free results obtained herein highlight the promise of this approach in providing predictive descriptions of the lattice thermal conductivity of materials.

DOI: 10.1103/PhysRevB.80.125203 PACS number(s): 66.70.−f, 63.20.kg, 71.15.Mb

I. INTRODUCTION

Diamond has the highest thermal conductivity, κ_L, of any known bulk material. Room-temperature values of κ_L for isotopically enriched diamond exceed 3000 W/m-K,[1–3] more than an order of magnitude higher than common semiconductors such as silicon and germanium. In diamond, the strong bond stiffness and light atomic mass produce extremely high phonon frequencies and acoustic velocities. In addition, the phonon-phonon umklapp scattering around room temperature is unusually weak. These properties result in the extremely large κ_L. The unusual thermal properties of diamond make it a particularly challenging test of any predictive theoretical approach used to describe it.

The mechanisms of phonon conduction in diamond and other crystalline semiconductors and insulators are well understood. Above a few tens of degrees Kelvin, phonon-phonon scattering typically becomes the dominant scattering mechanism that limits κ_L. This scattering process arises because of the anharmonicity of the interatomic potential. In addition, scattering of phonons by isotopic impurities reduces κ_L, and this effect can be tuned by varying the isotopic composition of the material.[1–3]

Many calculations of κ_L in semiconductors and insulators are based on a Boltzmann transport equation (BTE) approach. Development of a predictive quantum-mechanical approach is a formidable task because it requires (1) accurate microscopic descriptions of the harmonic and anharmonic interatomic forces in crystals and (2) an exact solution of the phonon BTE. Many theoretical treatments of phonon transport have employed single-mode phonon relaxation time approximations (RTAs).[4,5] For the case of phonon-phonon scattering the commonly used RTA form is of questionable validity because it was derived assuming low-frequency phonons at low temperature.[5] Also, RTAs are in principle incompatible with inelastic scattering processes such as phonon-phonon scattering.[4] Improved approximate solutions of the phonon Boltzmann equation have been achieved using variational approaches.[6,7] However, it is difficult to gauge the accuracy of these as they depend on the choice of trial functions used to represent the nonequilibrium distribution of phonons, and simple trial functions cannot be constructed that reflect the full anisotropic and nonlinear phonon dispersions characterizing most semiconductors.

More recently, an iterative approach to solve exactly the linearized phonon BTE has been achieved[8] and subsequently applied to bulk semiconductors[9–12] and to superlattices.[13,14] The only inputs to this approach are the harmonic and third-order anharmonic interatomic force constants (IFCs). In Refs. 9–11, 13, and 14, the IFCs have been introduced as parameters that have been adjusted to fit bulk thermal conductivity data.

Empirical interatomic potentials have been used in molecular dynamics simulations of thermal conductivity,[15,16] and in phonon BTE approaches.[12] However, these are time consuming to develop and are typically fit to only a small set of material properties such as lattice constants and cohesive energies. Consequently, empirical potentials are only available for a small number of already well-studied materials. Also, while the molecular dynamics approach, which is more appropriate at higher temperatures as the atomic motion is treated classically, has obtained more reasonable agreement with room-temperature κ_L for Si,[15] the phonon BTE approach for Si has shown poor agreement with experiment.[12] These factors motivate first-principles calculations of the IFCs, removing the necessity of adjustable parameters.

Over the last few decades, the density-functional theory (DFT) of Kohn and Sham[17] has developed into an extremely

accurate tool in the calculation of the electronic ground-state density of many structures. Derivatives of the ground-state total energy can be found through the use of density-functional perturbation theory (DFPT). The "2n+1" theorem[18] states that knowledge of the wave function response to n^{th} order in the strength of the external perturbation allows the calculation of the $(2n+1)^{th}$ energy derivative. This means that knowledge of the linear response of a crystal is sufficient to determine both harmonic and third-order anharmonic IFCs.

In a recent paper, we have developed a theoretical approach to calculate intrinsic lattice thermal conductivity free of adjustable parameters.[19] This approach combined an iterative solution of the phonon Boltzmann equation with harmonic and anharmonic IFCs obtained from *ab initio* DFPT calculations. Its application to silicon and germanium demonstrated excellent agreement with measured values of κ_L using no adjustable parameters. In this paper, we apply the method to study diamond. As discussed above, diamond has a significantly higher κ_L than silicon and germanium. Furthermore, its thermal conductivity is quite sensitive to isotopic impurity concentration.[1–3] As such, it provides a stringent test of our first-principles theoretical approach.

Section II of this paper describes the *ab initio* approach to calculate the harmonic and third-order anharmonic IFCs in the DFPT framework. Section III gives a brief description of the Boltzmann transport theory used to calculate the thermal conductivity. Section IV describes the computational details, Sec. V gives results along with a discussion, and Sec. VI provides a summary and conclusions.

II. INTERATOMIC FORCE CONSTANTS

The phonon frequencies and eigenvectors are solutions to the eigenvalue equation.

$$\sum_{\beta\kappa'} \frac{1}{\sqrt{M_\kappa M_{\kappa'}}} D_{\alpha\beta}(\kappa\kappa',\vec{q}) e_{\beta\kappa'}(\vec{q}) = \omega^2 e_{\alpha\kappa}(\vec{q}) \tag{1}$$

where $D_{\alpha\beta}$ is the reciprocal space dynamical matrix constructed from the real-space harmonic IFCs given by

$$D_{\alpha\beta}(\kappa\kappa',\vec{q}) = \sum_{l'} \Phi_{\alpha\beta}(0\kappa;l'\kappa') \exp(-i\vec{q}\cdot\vec{R}_{l'}) \tag{2}$$

with $\vec{R}_l$ being the position vector of the l^{th} unit cell, κ indicating the atom with mass M_κ within the l^{th} unit cell and the real-space harmonic IFCs being described by $\Phi_{\alpha\beta}$. The real-space harmonic IFCs are found by using the fast Fourier-transform technique on a set of reciprocal-space IFCs determined on an uniform grid in reciprocal space. The matrix of reciprocal-space harmonic IFCs is a combination of electronic and ionic parts and can be written

$$\tilde{\Phi}_{\alpha\beta}(\vec{q}) = \tilde{\Phi}^{el}_{\alpha\beta}(\vec{q}) + \tilde{\Phi}^{ion}_{\alpha\beta}(\vec{q}) = \frac{1}{N} \frac{\partial^2 E}{\partial u^{*\alpha}_\kappa \, \partial u^{\beta}_{\kappa'}} \tag{3}$$

where N is the number of unit cells. The ionic term involves the second derivative of the Ewald energy.[20]

The third-order anharmonic IFCs are evaluated first in reciprocal space, where they are given by the third-order derivatives of the total energy with respect to the Fourier transformed atomic displacements:[20,21]

$$\Phi^{\kappa\kappa'\kappa''}_{\alpha\beta\gamma}(\vec{q},\vec{q}',\vec{q}'') = \frac{\partial^3 E_{tot}}{\partial u^{\alpha}_{\kappa}(\vec{q}) \, \partial u^{\beta}_{\kappa'}(\vec{q}') \, \partial u^{\gamma}_{\kappa''}(\vec{q}'')}. \tag{4}$$

The "2n+1" theorem provides an analytic expression for these third-order anharmonic IFCs. The IFCs are symmetrical in the three sets of $\{\kappa,\alpha,\vec{q}\}$ and can be expanded into six terms,[21] each of which can be evaluated by the insertion of the projection operator, P_c on the unperturbed conduction states.[22] This leads to an expression that contains only terms that are accessible to 1st-order perturbation theory. Further details of this method are contained in Refs. 18, 21, and 22.

By using crystal symmetries, the $\Phi^{\kappa\kappa'\kappa''}_{\alpha\beta\gamma}$ are evaluated on a $4\times4\times4$ mesh for forty-two $\{\vec{q},\vec{q}'\}$ pairs (the $\vec{q}''$ is obtained from $\vec{q}''=\vec{q}\pm\vec{q}'+\vec{K}$ where $\vec{K}$ is a reciprocal lattice vector).[21] These IFCs are then transformed into real space with triplet interactions out to seventh nearest neighbors.

III. LINEARIZED BOLTZMANN EQUATION

The lattice thermal conductivities of diamond for different isotopic concentrations are calculated by means of Boltzmann transport theory. We begin by considering a small temperature gradient, ∇T, that perturbs the phonon distribution function, $n_\lambda = n^0_\lambda + n^1_\lambda$ where the shorthand $\lambda=(j,\vec{q})$ is used, n^0_λ is the Bose distribution function, and the nonequilibrium part, n^1_λ, is proportional to the small ∇T. We solve the linearized BTE

$$\vec{v}_\lambda \cdot \nabla T \frac{\partial n^0_\lambda}{\partial T} = \left.\frac{\partial n}{\partial t}\right|_c \tag{5}$$

where $\vec{v}_\lambda$ is the phonon velocity, and the collision term[4,8–12] describes the scattering into and out of the state, λ. The anharmonicity of the interatomic potential causes phonons to scatter inelastically from one another. Using the calculated phonon dispersions, the phase space of all possible three phonon scattering events that conserve both energy and crystal momentum is determined. Such processes must satisfy

$$\omega_j(\vec{q}) \pm \omega_{j'}(\vec{q}') = \omega_{j''}(\vec{q}'')$$

$$\vec{q} \pm \vec{q}' = \vec{q}'' + \vec{K} \tag{6}$$

Here, normal processes correspond to $\vec{K}=0$, while umklapp processes correspond to $\vec{K}\neq0$. Three-phonon scattering rates are computed from Fermi's golden rule with the anharmonic IFCs as an input

$$W^{\pm}_{\lambda\lambda'\lambda''} = \frac{\hbar\pi}{4N} \frac{(n^0_\lambda+1)\left(n^0_{\lambda'}+\frac{1}{2}\pm\frac{1}{2}\right)n^0_{\lambda''}}{\omega_\lambda\omega_{\lambda'}\omega_{\lambda''}} \times |\Phi^{\pm}_{\lambda\lambda'\lambda''}|^2 \delta(\omega_\lambda \pm \omega_{\lambda'} - \omega_{\lambda''}) \tag{7}$$

where ω_λ are the phonon frequencies. The three-phonon matrix element is given by

$$\Phi^{\pm}_{\lambda\lambda'\lambda''} = \sum_{\kappa}\sum_{l'\kappa'}\sum_{l''\kappa''}\sum_{\alpha\beta\gamma}\Phi_{\alpha\beta\gamma}(0\kappa,l'\kappa',l''\kappa'')e^{i\vec{q}'\cdot\vec{R}_{l'}} \times e^{i\vec{q}''\cdot\vec{R}_{l''}}\frac{e^{\lambda}_{\alpha\kappa}e^{\pm\lambda'}_{\beta\kappa'}e^{-\lambda''}_{\gamma\kappa''}}{\sqrt{M_\kappa M_{\kappa'}M_{\kappa''}}} \tag{8}$$

where the $\Phi_{\alpha\beta\gamma}(0\kappa,l'\kappa',l''\kappa'')$ are real-space anharmonic IFCs, and the $e^{\lambda}_{\alpha\kappa}$ are phonon eigenvectors, with $\lambda\rightarrow-\lambda\Rightarrow\vec{q}\rightarrow-\vec{q}$.

Isotopic impurities introduce elastic scattering of phonons. The scattering rate due to such impurities is calculated as[9,12]

$$W^{imp}_{\lambda\lambda'} = \frac{\pi}{2}g_2\omega_\lambda\omega_{\lambda'}n^0_\lambda(n^0_{\lambda'}+1)\sum_{\kappa}|\hat{e}^*_{\kappa\lambda}\cdot\hat{e}_{\kappa\lambda'}|^2\delta(\omega_{\lambda'}-\omega_\lambda). \tag{9}$$

Here g_2 is the mass variance parameter,[23] which describes the concentration and mass change for each isotope type.

These scattering rates are used in an iterative solution[8–12,19] of the linearized phonon BTE. Using the substitution, $n^1_\lambda = n^0_\lambda(n^0_\lambda+1)\beta\vec{F}_\lambda\cdot\nabla T$, the phonon BTE can be recast as:

$$F_{\lambda\alpha} = F^0_{\lambda\alpha} + \Delta F_{\lambda\alpha} \tag{10}$$

for Cartesian components $\alpha = x,y,z$, where

$$F^0_{\lambda\alpha} = \frac{\hbar\omega_\lambda n^0_\lambda(n^0_\lambda+1)v_{\lambda\alpha}}{TQ_\lambda} \tag{11}$$

and

$$\Delta F_{\lambda\alpha} = \frac{1}{Q_\lambda}\left\{\sum_{\lambda'\lambda''}\left[W^{+}_{\lambda\lambda'\lambda''}(F_{\lambda''\alpha}-F_{\lambda'\alpha}) + \frac{1}{2}W^{-}_{\lambda\lambda'\lambda''}(F_{\lambda''\alpha}+F_{\lambda'\alpha})\right]\right\} \tag{12}$$

and the total scattering rate is

$$Q_\lambda = \sum_{\lambda'\lambda''}\left(W^{+}_{\lambda\lambda'\lambda''}+\frac{1}{2}W^{-}_{\lambda\lambda'\lambda''}\right)+\sum_{\lambda'}W^{imp}_{\lambda\lambda'}. \tag{13}$$

We consider a temperature gradient along the [001] (z) direction. The iterative procedure begins by setting $F'_{\lambda z}=F''_{\lambda z}=0$. The resulting zeroth-order solution, Eq. (11), is equivalent to a single mode RTA.[4,5] This solution is inserted into the right-hand side of Eq. (12) to obtain the first-order solution. The iteration procedure is repeated until convergence is achieved. The phonon scattering time is related to $F_{\lambda z}$ as $\tau_{\lambda z}=TF_{\lambda z}/\hbar\omega_\lambda v_{\lambda z}$. It is used to calculate the lattice thermal conductivity as

$$\kappa_{zz} = \frac{1}{V}\sum_{\lambda}C_\lambda v_z^2\tau_{\lambda z} \tag{14}$$

where $C_\lambda = k_B n^0_\lambda(n^0_\lambda+1)(\hbar\omega_\lambda\beta)^2$ is the specific heat per mode, $\beta = 1/(k_BT)$, and V is the crystal volume.

A key feature of the above described approach is that the only inputs are the lattice constant, harmonic, and third-order anharmonic IFCs obtained within the DFPT framework without the need for any empirical parameters as discussed in Sec. II, and the mass variance parameter, which is obtained from the experimentally determined isotopic impurity concentration. The harmonic IFCs are required for calculation of the phonon frequencies and eigenvectors, the anharmonic IFCs are used in the calculation of the phonon-phonon scattering rates.

IV. COMPUTATIONAL DETAILS

All ground-state energies and harmonic IFCs were calculated using the Quantum Espresso program.[24] The anharmonic IFCs were generated following the method described in Ref. 21.

The ion-electron interaction and exchange-correlation effects are modeled in the framework of pseudopotential theory. For diamond, we have used the BHS pseudopotential,[25] for both harmonic and anharmonic IFCs. This pseudopotential was constructed from all-electron calculations ensuring that the parameter-less nature of the calculations is preserved. The exchange-correlation energy is calculated in the framework of the local-density approximation (LDA) using the results of Ceperley and Alder[26] as parameterized by Perdew and Zunger.[27]

Mode Grüneisen parameters provide an important measure of the anharmonicity of the crystal. They describe the change in the phonon-mode frequency with crystal volume by

$$\gamma_\lambda = -\frac{V}{\omega_\lambda}\frac{\partial\omega_\lambda}{\partial V}. \tag{15}$$

The mode Grüneisen parameter can also be expressed in terms of the third-order anharmonic IFCs (Refs. 12, 28, and 29)

$$\gamma_\lambda = -\frac{1}{6\omega^2_\lambda}\sum_{\kappa}\sum_{l'\kappa'}\sum_{l''\kappa''}\sum_{\alpha\beta\gamma}\Phi_{\alpha\beta\gamma}(0\kappa,l'\kappa',l''\kappa'') \times\frac{e^{\lambda*}_{\alpha\kappa}e^{\lambda}_{\beta\kappa'}}{\sqrt{M_\kappa M_{\kappa'}}}e^{i\vec{q}\cdot\vec{R}_{l'}}\vec{r}_{l''\kappa''\gamma}. \tag{16}$$

Where $\vec{r}_{l\kappa\gamma}$ is the γ^{th} component of the vector describing the position of the κ^{th} atom in the l^{th} unit cell. The linear expansion coefficients can be obtained as a sum of the γ_λ over all modes weighted by the mode-specific heat[29]

$$\alpha = \frac{\kappa_T}{3V}\sum_{\lambda}C_\lambda\gamma_\lambda \tag{17}$$

where κ_T is the isothermal compressibility.

We have used the calculated linear expansion coefficient to establish the cut-off energy for the plane-wave basis. Calculations of $\alpha(T)$ were performed as a function of temperature for successively higher cut-off energies. Convergence was achieved at 100 Ry and so this cut-off energy was used for diamond.

The harmonic IFCs were calculated using a $6\times6\times6$ Monkhorst-Pack[30] q-point mesh. A $4\times4\times4$ Monkhorst-

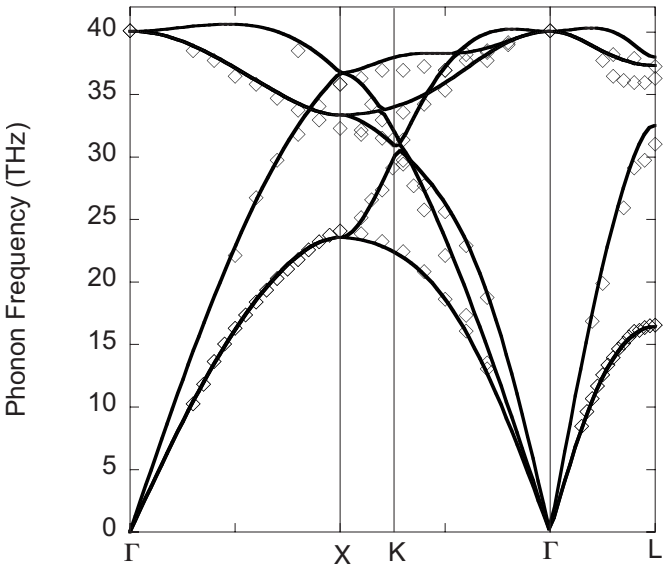

FIG. 1. Phonon dispersions of diamond. *Ab initio* calculations (solid line) and experiment (open diamonds).

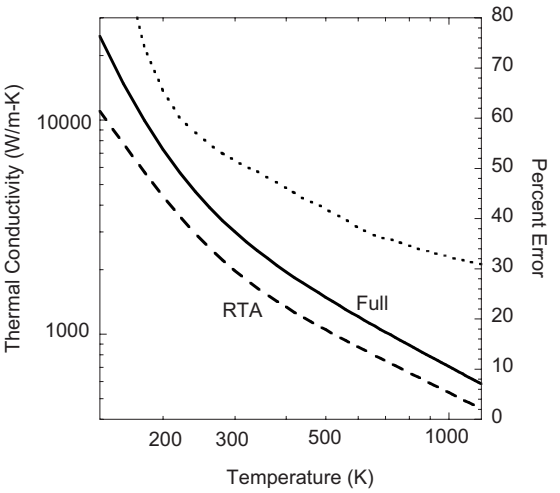

FIG. 2. The calculated intrinsic lattice thermal conductivity of diamond for the RTA (dashed line) and the full converged solution (solid line). Dotted line shows percent error of the RTA result compared to the full solution.

Pack k-point mesh was used in determining the anharmonic IFCs. The anharmonic IFCs were calculated considering interactions out to seventh nearest neighbors.[21] The lattice constant that minimized the ground-state energy for diamond was found to be 6.675 Bohr. This value is less than the experimental value of 6.74 Bohr as expected, as it is well known that *ab initio* methods in the LDA formalism "overbind" leading to smaller lattice constants.

To test the consistency of the harmonic and anharmonic IFCs, Eqs. (15) and (16) were used to evaluate the mode Grüneisen parameters throughout the Brillouin zone. Excellent agreement was obtained between the two sets of results.

For each temperature, κ_L was calculated using the iterative solution to the phonon Boltzmann equation as outlined in Sec. IV and incorporating *ab initio* IFCs described in Sec. III. The phase space search for all allowed phonon-phonon scattering events was performed on a Gaussian quadrature grid for all three components of $\vec{q}$ and the x and y component of $\vec{q}'$. The z component of $\vec{q}'$ was chosen from a finer linear grid.

The final calculations were performed using a 32 point GAUSSIAN quadrature for each q component and a maximum of 200 points in the linear q_z' grid.

The thermal conductivity calculation proceeds by calculating a zeroth-order solution and then iterating until convergence is achieved. For higher temperatures, of the order of 30 iterations are performed to achieve convergence. At lower temperatures, more iterations are required. The large Debye temperature of diamond ($\sim$2200 K) means that 300 K can be considered low temperature. Also, the umklapp scattering is exceedingly weak. Both of these facts lead to around 50 iterations for convergence in diamond.

V. RESULTS AND DISCUSSION

The remarkable accuracy of *ab initio* plane-wave pseudopotential calculations within the LDA formalism at calculating lattice dynamical properties of semiconductors is well documented.[20,31] For completeness, the diamond phonon dispersions calculated from the DFPT generated harmonic IFCs are compared with experiment[32] in Fig. 1. The high degree of agreement between the theory and experiment is clear.

In Fig, 2, the calculated intrinsic lattice thermal conductivity (g_2=0) of diamond is plotted as a function of temperature. The dashed line shows the RTA (zeroth order) result, κ_0, while the solid line, κ_L, is obtained from the full iterated solution to the phonon Boltzmann equation. It is evident from the figure that the RTA solution gives a poor approximation to the lattice thermal conductivity of diamond. For example, at 300 K, κ_L is about 50% higher than κ_0.

To understand the reason for this, we note that if there is no umklapp (U) scattering, κ_L must diverge because normal (N) scattering cannot provide thermal resistance. This divergence does not occur in the RTA (zeroth-order solution) because in this approximation, the N and U processes are independent and both enter in a purely resistive manner in the total scattering rate, Eq. (7). When only N processes are included, the lack of thermal resistance manifests itself through the iterative procedure. With increasing number of iterations the solution of Eq. (10) approaches $F_{\lambda z}=\Delta F_{\lambda z}$, which corresponds to a vanishing of the collision term in the phonon BTE. This means that a flowing phonon current can exist in the absence of a temperature gradient. In this case, the calculated thermal conductivity diverges.

In materials such as Si and Ge, the U scattering is strong so the behavior of κ_L is dominated by this U scattering. In such cases, we find that the converged solution to the phonon BTE is less than 10% higher than the RTA solution. In diamond, however, the U scattering is considerably weaker than in Si or Ge. This is reflected in the dramatically smaller phase space for three-phonon scattering for diamond as compared to other materials.[33] The dominance of N scattering in diamond has been noted previously.[2,3,34] Here, this dominance manifests itself through the converged solution of the phonon BTE giving a κ_L that lies far higher than the RTA

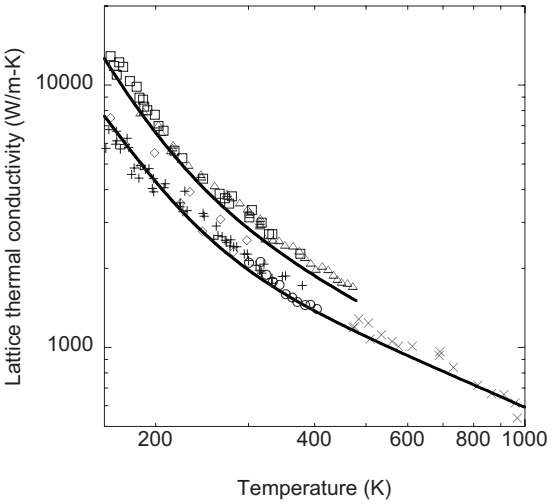

FIG. 3. Lattice thermal conductivity of isotopically enriched and naturally occurring diamond as a function of temperature. Measured values (open triangles, squares, open diamonds, open circles, and crosses) are compared with the results of *ab initio* calculations (solid lines).

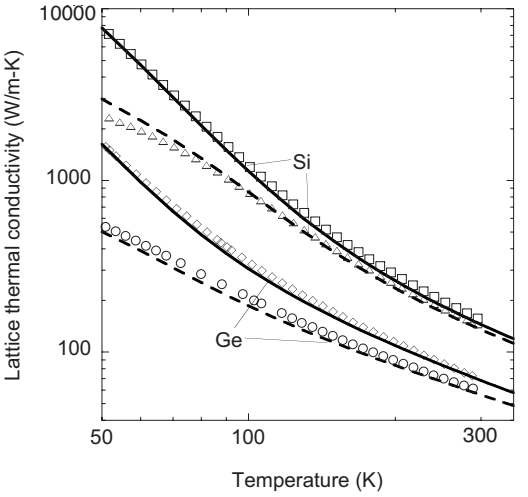

FIG. 4. Lattice thermal conductivity of naturally occurring (dashed lines) and isotopically enriched (solid lines) Si and Ge as a function of temperature compared with the corresponding experimental values.

solution, as can be seen in Fig. 2. Note that the percent error (dotted curve) increases with decreasing temperature. This is to be expected since decreasing T further weakens the umklapp scattering.

Figs. 3 compares the lattice thermal conductivity of isotopically enriched and naturally occurring diamond as a function of temperature obtained from our *ab initio* approach with experimentally measured values. The open squares[2] and triangles[3] show the measured values for isotopically enriched diamond with 99.93% C^{12}, 0.07% C^{13}, 99.9% C^{12}, and 0.1% C^{13}, respectively. The open diamonds,[35] open circles,[1] plusses,[3] and crosses[2] are for naturally occurring type IIa diamond with 98.9% C^{12} and 1.1% C^{13}. The mass variance parameters obtained from the isotopic compositions are given in Table I. The corresponding calculated results using the IFCs discussed in Sec. IV is given by the solid curves. It is evident that the calculated curves for both the isotopically enriched and naturally occurring diamond are in very good overall agreement with the data, lying within 10%–15% of the measured values over the wide temperature range considered. This agreement is particularly impressive since there are no adjustable parameters.

Previously, the intrinsic lattice thermal conductivities of Si and Ge were calculated using the *ab initio* approach described here.[19] In the present paper, those results are extended to include the effect of isotope scattering. Naturally occurring Si consists of 92.2% Si^{28}, 4.7% Si^{29}, and 3.1% Si^{30}, while naturally occurring Ge[23] has 20.5% Ge^{70}, 27.4% Ge^{72}, 7.8% Ge^{73}, 36.5% Ge^{74}, and 7.8% Ge^{76}. The isotopically enriched samples have 99.983% Si^{28}, 0.014% Si^{29}, 0.003% Si^{30}, and 99.99% Ge^{70} and 0.01% Ge^{73}.

TABLE I. Mass variance parameters for isotopically enriched and naturally occurring diamond, Si and Ge.

	Naturally occurring	Isotopically enriched
Diamond	7.54×10^{-5}	4.86×10^{-6}
Si	2.01×10^{-4}	2.33×10^{-6}
Ge	5.89×10^{-4}	8.16×10^{-8}

Fig. 4 shows the lattice thermal conductivity of naturally occurring (dashed curves) and isotopically enriched (solid curves) Si and Ge compared with the corresponding experimental values.[36,37] The agreement between theory and experiment is extremely good for both the naturally occurring and isotopically enriched Si and Ge. As the temperature increases, the calculations for the naturally occurring and isotopically pure samples converge because the U scattering becomes stronger with increasing temperatures and consequently drives the thermal conductivity. It is evident that the isotope effect is larger in Ge than Si. This is a consequence of the spread of isotopes in the naturally occurring Ge, which gives a larger g_2.

In our calculations, we have taken the lattice constant to be given by its zero-temperature value. For higher temperatures, thermal expansion causes the lattice constant to increase. Thus, in principle, the lattice constant and corresponding IFCs should be found by minimizing the Helmholtz free energy at each temperature.[38] We have investigated the effect of lattice constant changes by calculating κ_L using IFCs determined using larger lattice constants representative of the higher temperatures. We find for Si, Ge, and diamond that κ_L is relatively insensitive to such changes. For example, for diamond the room temperature value of κ_L drops by only 1% when the lattice constant increases by 0.4% from its zero temperature calculated value of 6.675 to 6.70 Bohr. Such a percentage change in lattice constant would correspond to a temperature change from 0 K to around 1000 K.[38]

The g_2 in diamond is considerably smaller than in either Si or Ge, but its isotope effect is larger. This is a consequence of the much weaker U scattering in diamond compared to Si and Ge. Because of this, the phonon scattering time, $\tau_{\lambda z}$, for isotopically pure diamond becomes very large

TABLE II. Zone center frequencies, $\omega_{LO}(\Gamma)$, transverse (TA), and longitudinal acoustic (LA) velocities, v_{TA} and v_{LA} and three-phonon phase space, P_3, for Si, Ge, and diamond.

	$\omega_{LO}(\Gamma)$ (THz)	v_{TA} (m/s)	v_{LA} (m/s)	P_3 (10^{-2})
Si	15.49	5413	8216	0.3536
	(15.5)[39]	(5843)[40]	(8420)[40]	
Ge	8.92	3251	4844	0.5795
	(9.02)[41]	(3542)[42]	(4914)[42]	
Diamond	39.17	12567	17326	0.0796
	(40.11)[32]	(12830)[43]	(17520)[44]	

at low frequency as the behavior is governed by N scattering processes. Introduction of isotopic impurities more strongly suppresses the low-frequency $\tau_{\lambda z}$ in diamond than in Si or Ge. This behavior has been noted previously.[34]

That κ_L of diamond is significantly larger than for the other group IV materials is due the strong bond stiffness and light mass of carbon, which produce extremely high phonon frequencies and acoustic velocities. These quantities enter directly in the thermal conductivity integral, Eq. (14), and so contribute to increasing κ_L for diamond compared to other materials. However, we have found that there is an inverse relationship between the phonon frequency/acoustic velocity scale and the phase space for phonon-phonon scattering. We can define a dimensionless fraction, P_3, that measures the availability of actual energy- and momentum-conserving three-phonon scattering processes governed by Eq. (6) relative to a hypothetical unrestricted space.[33] The much higher phonon-frequency scale in diamond results in a dramatic reduction in the phase space for phonon-phonon scattering. As a result, there are far fewer resistive scattering processes to limit κ_L. Table II lists the calculated maximum phonon frequencies, $\omega_{LO}(\Gamma)$, transverse (TA), and longitudinal acoustic (LA) velocities, v_{TA} and v_{LA}, along the [100] direction (the experimental values appear in parentheses) and the three-phonon phase space, P_3, for Si, Ge and diamond. It is evident that diamond has significantly higher $\omega_{LO}(\Gamma)$, v_{TA}, and v_{LA}, but a considerably lower P_3 than both Si and Ge.

To further illustrate this point, the thermal conductivities of two isotopically pure hypothetical materials, A and B are investigated. For material A, the calculated diamond velocities and frequencies are combined with the scattering times, $\tau_{\lambda z}$, for Si in calculating the thermal conductivity from Eq. (14). For material B, the opposite combination is used. In this way, the importance of the frequency/velocity scale in the one material is weighed against the phonon-phonon scattering phase space availability in the other. We find the calculated room-temperature thermal conductivities for materials A and B to be 712 W/m-K and 1021 W/m-K, respectively. These values lie squarely between those calculated for isotopically pure Si (145 W/m-K) and diamond (2966 W/m-K). It is clear that the large phonon frequencies and acoustic velocities in diamond cannot alone account for its significantly larger thermal conductivity compared to Si. The reduction in the phase space for phonon-phonon scattering also plays an important role.

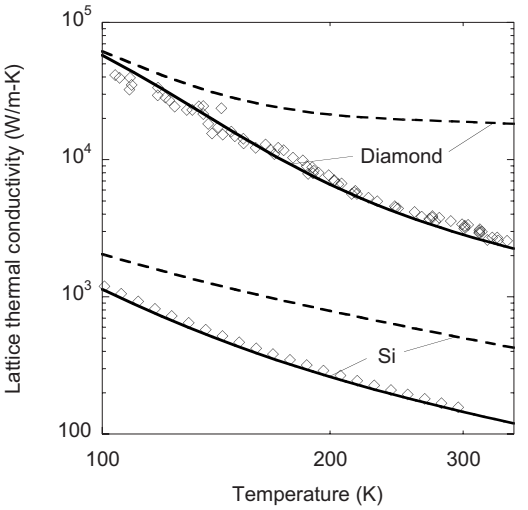

FIG. 5. Isotopically enriched lattice thermal conductivity of diamond and Si from the full calculations (solid lines) and for the case where the acoustic-optic phonon-phonon scattering channels have been omitted (dashed lines). Measured values for isotopically enriched diamond and Si are also included.

In most calculations of the lattice thermal conductivity, optic phonons are not included. This is because optic phonons have small group velocities, so there is little direct contribution to κ_L from the integral over the three optic phonon branches. It is certainly the case that the heat-carrying acoustic phonons account for the majority of the thermal current. However, the optic phonons provide essential scattering channels for the acoustic phonons.[9,10,19] In order to illustrate this, we have calculated the lattice thermal conductivities of isotopically enriched diamond and Si as a function of temperature with all scattering processes between acoustic and optic phonons removed. Figure 5 shows the results of these calculations. The solid lines give results of the full calculations for isotopically enriched diamond (Si) already shown in Figs. 3 and 4. The experimental data for isotopically enriched diamond[1–3] and Si[36] are included for completeness. The dashed lines give the results with the acoustic-optic scattering omitted. For Si, κ_L exhibits a large jump, showing more than a threefold increase at room temperature. For diamond, removal of the acoustic-optic scattering produces an even more striking increase with more than a sixfold increase at room temperature. This occurs because the phase space for three-phonon scattering in diamond is extremely small and around 80% of the energy and momentum conserving processes that contribute to the total scattering rates for the acoustic branches involve optic phonons. For both materials, the gap between the two cases increases with temperature. This behavior is a result of the fact that the population of optic phonons increases with temperature thereby enhancing the acoustic-optic phonon scattering rates. It is interesting that as the temperature increases, the temperature dependence of the diamond thermal conductivity without acoustic-optic phonon scattering becomes weaker. This reflects the fact that for this case, the isotopic impurity scattering is an important scattering mechanism, and it has no temperature dependence. In contrast, for Si, the thermal

conductivity is still dominated by three-phonon scattering even when acoustic-optic scattering have been removed, and this is reflected in the stronger temperature dependence of the dashed curve for Si in Fig. 5.

We note that in Ref. 10, a much smaller increase of the lattice thermal conductivity of diamond was found when the acoustic-optic phonon scattering channels were removed. There, only an increase by a factor of 1.2 (2) was obtained at 200 K (500 K), considerably less that found in the present work. One possible explanation of this is that in Ref. 10, a short-ranged central potential model was used. The central potential parameters fit to the diamond dispersions give acoustic velocities that are considerably lower than the experimental values (see Fig. 1 of Ref. 10). In such a case, the energy conservation condition in Eq. (6) would cause the phase space for three-phonon scattering to be weighted more heavily by *aaa* scattering so that removal of the acoustic-optic phonon scattering (*aao* and *aoo*) would have a weaker effect. Our *ab initio* approach gives phonon dispersions that are in excellent agreement with measured values (see Fig. 1), and from it, we find only about 20% of the three-phonon scattering events to involve three acoustic phonons, as stated above. The large increase in thermal conductivity displayed in Fig. 5 when acoustic-optic phonon scattering is removed is consistent with this result.

VI. SUMMARY AND CONCLUSIONS

We have calculated the lattice thermal conductivity of diamond using an *ab initio* DFPT approach for the harmonic and anharmonic IFCs combined with an exact solution of the linearized phonon BTE. This approach has predictive capability since it introduced no adjustable parameters. We have found very good agreement with the measured diamond thermal conductivity over a wide temperature range for both isotopically enriched and naturally occurring diamond. Similarly good agreement has been demonstrated for isotopically enriched and naturally occurring Si and Ge. We have demonstrated that the commonly used relaxation time approximation provides a poor representation of the actual solution to the BTE for diamond because of the weak umklapp scattering.

We have also highlighted the importance of including scattering between acoustic and optic phonons in properly representing the lattice thermal conductivity of materials. The sensitivity of the thermal conductivity to acoustic-optic phonon-phonon scattering has been the subject of a previous experimental investigation of III-V materials.[45] In that work, it was demonstrated that III-V materials with larger energy gaps between acoustic and optic phonon branches showed higher scaled thermal conductivities. This result was attributed to the decreased scattering between acoustic and optic phonons. It has also been suggested recently[46] that the low-lying optic phonon branch in PbTe could explain its anomalously low-thermal conductivity. Here we provide quantitative evidence for this effect. These results suggest that the ability to tune the frequencies of the optic phonons would provide a means to tailor the lattice thermal conductivity of materials.

We note that first-principles studies of structural, vibrational and thermodynamic properties of diamond have also demonstrated excellent agreement with experiment.[38,47] In addition, recent *ab initio* studies of phonon linewidths in Si and Ge,[21] and phonon properties and transport in graphene, graphite, and nanotubes[48–51] have been performed. Such studies along with the present work highlight the promise of developing predictive first-principles based theories to describe a wide range of material properties.

ACKNOWLEDGMENTS

The authors gratefully acknowledge support from the National Science Foundation under Grant No. CBET 0651381 and No. 0651427. Part of this work was done on the Intel Computing Cluster at the Cornell Nanoscale Facility, part of the National Nanotechnology Infrastructure Network supported by the National Science Foundation. We also acknowledge computational support from the Boston College computing cluster. One of us (D.A.B.) acknowledges useful discussions with Joseph Heremans.

[1] D. G. Onn, A. Witek, Y. Z. Qiu, T. R. Anthony, and W. F. Banholzer, Phys. Rev. Lett. **68**, 2806 (1992).
[2] J. R. Olson, R. O. Pohl, J. W. Vandersande, A. Zoltan, T. R. Anthony, and W. F. Banholzer, Phys. Rev. B **47**, 14850 (1993).
[3] L. Wei, P. K. Kuo, R. L. Thomas, T. R. Anthony, and W. F. Banholzer, Phys. Rev. Lett. **70**, 3764 (1993).
[4] J. M. Ziman, *Electrons and Phonons* (Oxford University Press, London, 1960).
[5] P. G. Klemens, in *Solid State Physics*, edited by F. Seitz and D. Turnbull (Academic Press, New York, 1958), Vol. 7.
[6] S. Pettersson, J. Phys. C **20**, 1047 (1987).
[7] S. Pettersson, Phys. Rev. B **43**, 9238 (1991).
[8] M. Omini and A. Sparavigna, Phys. Rev. B **53**, 9064 (1996).
[9] M. Omini and A. Sparavigna, Nuovo Cimento D **19**, 1537 (1997).
[10] A. Sparavigna, Phys. Rev. B **65**, 064305 (2002).
[11] A. Sparavigna, Phys. Rev. B **66**, 174301 (2002).
[12] D. A. Broido, A. Ward, and N. Mingo, Phys. Rev. B **72**, 014308 (2005).
[13] D. A. Broido and T. L. Reinecke, Phys. Rev. B **70**, 081310 (2004).
[14] A. Ward and D. A. Broido, Phys. Rev. B **77**, 245328 (2008).
[15] S. G. Volz and G. Chen, Phys. Rev. B **61**, 2651 (2000).
[16] P. K. Schelling, S. R. Phillipot, and P. Keblinski, Phys. Rev. B **65**, 144306 (2002).
[17] W. Kohn and L. J. Sham, Phys. Rev. **140**, A1133 (1965).
[18] X. Gonze and J. P-. Vigneron, Phys. Rev. B **39**, 13120 (1989).
[19] D. A. Broido, M. Malorny, G. Birner, N. Mingo, and D. A. Stewart, Appl. Phys. Lett. **91**, 231922 (2007).
[20] P. Giannozzi, S. di Gironcoli, P. Pavone, and S. Baroni, Phys.

Rev. B **43**, 7231 (1991).
[21] G. Deinzer, G. Birner, and D. Strauch, Phys. Rev. B **67**, 144304 (2003).
[22] A. Debernardi and S. Baroni, Solid State Commun. **91**, 813 (1994).
[23] M. Asen-Palmer, K. Bartkowski, E. Gmelin, M. Cardona, A. P. Zhernov, A. V. Inyushkin, A. Taldenkov, V. I. Ozhogin, K. M. Itoh, and E. E. Haller, Phys. Rev. B **56**, 9431 (1997).
[24] S. Baroni *et al.*, http://www.quantum-espresso.org.
[25] G. B. Bachelet, D. R. Hamann, and M. Schlüter, Phys. Rev. B **26**, 4199 (1982).
[26] D. M. Ceperley and B. J. Alder, Phys. Rev. Lett. **45**, 566 (1980).
[27] J. Perdew and A. Zunger, Phys. Rev. B **23**, 5048 (1981).
[28] T. H. K. Barron and M. L. Klein, in *Dynamical Properties of Solids*, edited by G. K. Horton and A. A. Maradudin (North-Holland, Amsterdam, 1974), Vol. I, p. 391.
[29] J. Fabian and P. B. Allen, Phys. Rev. Lett. **79**, 1885 (1997).
[30] H. J. Monkhorst and J. D. Pack, Phys. Rev. B **13**, 5188 (1976).
[31] M. T. Yin and M. L. Cohen, Phys. Rev. B **26**, 3259 (1982).
[32] J. L. Warren, J. L. Yarnell, G. Dolling, and R. A. Cowley, Phys. Rev. **158**, 805 (1967).
[33] L. Lindsay and D. A. Broido, J. Phys.: Condens. Matter **20**, 165209 (2008).
[34] R. Berman, Phys. Rev. B **45**, 5726 (1992).
[35] R. Berman, P. R. W. Hudson, and M. Martinez, J. Phys. C: Solid State Phys. **8**, L430 (1975).
[36] A. V. Inyushkin, A. N. Taldenkov, A. M. Gibin, A. V. Gusev, and H.-J. Pohl, Phys. Status Solidi C **1**, 2995 (2004).
[37] V. I. Ozhogin, A. V. Inyushkin, A. N. Taldenkov, A. V. Tikhomirov, and G. E. Popov, JETP Lett.Phy **63**, 490 (1996).
[38] N. Mounet and N. Marzari, Phys. Rev. B **71**, 205214 (2005).
[39] G. Dolling, *Proc. Symp. Inelastic Scattering Neutrons in Solids and Liquids* (IAEA, Vienna, 1963), Vol. 2, p. 37.
[40] H. J. McSkimin, J. Appl. Phys. **24**, 988 (1953).
[41] G. Nilsson and G. Nelin, Phys. Rev. B **6**, 3777 (1972).
[42] H. J. McSkimin and P. Andreatch, Jr., J. Appl. Phys. **34**, 651 (1963).
[43] H. J. McSkimin, P. Andreatch, Jr., and P. Glynn, J. Appl. Phys. **43**, 985 (1972).
[44] Online archive on physical properties of semiconductors at www.ioffe.ru/sva/nsm/semicond/index.html.
[45] E. F. Steigmeier and I. Kudman, Phys. Rev. **141**, 767 (1966).
[46] J. An, A. Subedi, and D. J. Singh, Solid State Commun. **148**, 417 (2008).
[47] P. Pavone, K. Karch, O. Schütt, W. Windl, D. Strauch, P. Giannozzi, and S. Baroni, Phys. Rev. B **48**, 3156 (1993).
[48] N. Bonini, M. Lazzeri, N. Marzari, and F. Mauri, Phys. Rev. Lett. **99**, 176802 (2007).
[49] N. Bonini, R. Rao, A. M. Rao, N. Marzari, and J. Menéndez, Phys. Status Solidi **245**, 2149 (2008).
[50] I. Savic, N. Mingo, and D. A. Stewart, Phys. Rev. Lett. **101**, 165502 (2008).
[51] D. A. Stewart, I. Savic, and N. Mingo, Nano Lett. **9**, 81 (2009).